Geotech Geol Eng (2024) 42:5209–5228
https://doi.org/10.1007/s10706-024-02837-x

ORIGINAL PAPER

Prediction of Excess Pore Water Pressure Generation in Sand–Silt Mixtures During Cyclic Loading: A Dissipated Energy-Based Model

Mohammad Hassan Baziar · **Mohammad Hossein Mollahassani Lashkajani**

Received: 8 January 2024 / Accepted: 21 May 2024 / Published online: 18 June 2024

Abstract This study investigates the effect of non-plastic fines content of sand–silt mixtures on excess pore water pressure generation using an energy-based approach. For this purpose, an experimental program was designed and conducted on mixtures of Firoozkuh sand No. 161 and Firoozkuh silt. A total of 35 undrained strain-controlled cyclic triaxial tests were performed on the reconstituted specimens of sand–silt mixtures, with a wide range of effective parameters such as relative density, effective confining stress, and fines content. Also, to present a more generalized and precise model, 37 undrained cyclic tests were collected from previous studies. Then, using nonlinear regression analysis and the results of these 72 tests, a model, relating residual excess pore water pressure ratio (r_u) to the ratio of dissipated energy to capacity energy (W/W_{liq}), is proposed. The results indicated that initial effective confining stress has a negligible effect on the $r_u - W/W_{liq}$ trend and so, the calibration parameter of the model only depends on the relative density and fines content. Convincingly, the accuracy of the proposed model was verified using the results of a series of centrifuge tests, reported by others, and the recorded data of wildlife downhole array site during the Superstition Hills 1987 earthquake. The proposed model is practical, applicable to various sands and sand–silt mixtures with nonplastic fines contents, and able to be calibrated using convenient parameters (i.e., relative density and fines content). Finally, the model can be easily implemented in site response analysis for energy-based liquefaction potential evaluation.

Keywords Sand–silt mixture · Prediction model · Residual pore water pressure · Dissipated energy · Non-plastic silt

M. H. Baziar (✉) · M. H. Mollahassani Lashkajani
School of Civil Engineering, Iran University of Science and Technology (IUST), Narmak, Tehran, Iran
e-mail: Baziar@iust.ac.ir

M. H. Mollahassani Lashkajani
e-mail: mh_mollahasani@civileng.iust.ac.ir

1 Introduction

Liquefaction and its consequences always have been a great concern of geotechnical and earthquake engineers. Cyclic strains induced by earthquake tend to rearrange the soil particles, and in undrained condition leads to build up excess pore water pressure (EPWP). Increasing pore water pressure can cause a severe reduction in soil strength and stiffness. Such EPWP generation has a significant effect on the stability of geotechnical structures and settlement characteristics of a soil deposit, even if it does not cause the soil to fully liquefy (Hazirbaba and Rathje 2009; Chen et al. 2019).

The stress-based method (SBM) is the most commonly used method for liquefaction potential evaluation in engineering practice. In this method, the cyclic resistance ratio (CRR)-the amplitude of cyclic loading with a specified number of cycles that soil can resist up to liquefaction- is compared with the cyclic stress ratio (CSR) induced by the design earthquake. Therefore, earthquake random loading should be converted to an equivalent harmonic loading with proper amplitude and specified number of cycles.

As an alternative, the energy-based method (EBM) is developed based on the early work of Nemat-Nasser and Shokooh (1979) who showed that dissipated energy per unit volume of soil during the cyclic loading is proportioned with EPWP generation. The dissipated energy is equal to cumulative area bounded by the stress–strain hysteresis loops. In the EBM method, the factor of safety (FS) against liquefaction is defined as the ratio of dissipated energy required for the onset of liquefaction (capacity energy, W_{liq}) to the amount of energy imparted to the soil by the energy source (earthquake, blast, etc.), known as demand energy. If the demand energy exceeds the capacity energy (FS < 1), then the soil liquefies.

Many researches demonstrated that there is a unique relationship between EPWP generation and dissipated energy regardless of the stress–strain path (e.g., Liang 1995; Tao 2003; Kokusho and Kaneko 2018; Baziar et al. 2019; Zhou et al. 2023; Sezer et al. 2024). Also, the EBM can simultaneously consider the effect of both stress and strain time histories on the liquefaction behavior of soil. Therefore, due to the irregularities of earthquake motions, using EBM for liquefaction evaluation is more sound and convenient compared to the SBM.

Kokusho (2013) and Kokusho (2017) addressed the advantages of EBM over SBM to assess liquefaction potential and developed a procedure for the determination of demand energy imparted to the soil by upward seismic waves. Kokusho and Tanimoto (2021) performed a series of cyclic triaxial tests on intact soil specimens and showed that there is a correlation between capacity energy (W_{liq}) and cyclic resistance ratio (CRR) irrespective of soil relative density, fines content, plasticity, and aging. Therefore, capacity energy (W_{liq}) can be determined using the conventional correlation of CRR in SBM, regardless of soil types. Baziar and Rostami (2017) presented an attenuation model to estimate demand energy at a site based on earthquake characteristics and site effects. These aforementioned studies facilitate the use of EBM in engineering practice, but there is still a lack of an efficient and simple EBM model for EPWP generation.

Several energy-based EPWP models were proposed by previous researchers using cyclic test results which had insufficient variations of parameters such as initial relative density (D_r), effective confining stress (σ'_m), and fines content (FC) (e.g., Yanagisawa and Sugano 1994; Wang et al. 1997; Polito et al. 2008; Jafarian et al. 2012). The model presented by Polito et al. (2008), is the only available energy-based EPWP model which takes into account the effect of fines content as a key parameter. However, this model, similar to the other proposed models, relates the residual EPWP ratio (r_u) to the dissipated energy (W) and cannot be efficient for different types of soils, while the capacity energy is influenced by many factors (such as effective confining stress, relative density, soil gradation, etc.) and can vary significantly in amount (Baziar and Jafarian 2007). On the other hand, the model proposed by Jafarian et al. (2012) relates the r_u to the energy ratio (W/W_{liq}), dissipated energy normalized by the capacity energy, which makes it more accurate in predicting r_u for different soil types. However, this model originally was developed based on cyclic test results of clean sand and cannot properly predict the EPWP generation in sand–silt mixtures.

Natural deposits usually contain different amounts of fines and many studies have shown that the fines content has a considerable effect on the liquefaction behavior of sand–silt mixtures (e.g., Polito 1999; Polito et al. 2008; Hazirbaba and Rathje 2009; Baziar et al. 2011; Porcino and Diano 2017; Akhila et al. 2019; Doygun et al. 2019; Porcino et al. 2020; Liu 2020; Gobbi et al. 2021; Ghani and Kumari 2021; Cheng and Zhang 2024). The present study aims to develop an efficient EPWP model based on the dissipated energy and related key parameters including relative density, silt content, and effective confining stress. For this purpose, a series of cyclic triaxial tests with variations of related parameters were performed. Moreover, a series of cyclic tests results were collected from previous studies for the present research. Then, all the performed and collected tests results were analyzed using the energy approach to develop a model for the prediction of EPWP generation in sand–silt mixtures. Furthermore, the proposed model was verified using three centrifuge tests and one field case study.

2 Experimental Program

To investigate the pore water pressure generation trend in clean sand and sand–silt mixture, a series of 35 strain-controlled undrained cyclic triaxial tests were performed on the samples with seven different fines contents (0, 10, 20, 30, 50, 70 and, 100 percent), four target relative densities of 20, 40, 60 and 80% and three effective confining stresses of 50, 100 and 200 kPa.

2.1 Materials

The tested sand in this study was Firoozkuh No. 161, synthetic crushed silica sand with similar properties as Toyoura sand which has been used by many researchers in Iran. Firoozkuh No. 161 can be considered as a medium to fine uniform clean sand (less than 0.5% fines content), having golden to yellow color and subangular to subrounded shape and is classified as SP (poorly graded sand) according to the Unified Soil Classification System (USCS). The silt used in this study was Firoozkuh silt from the same origin as Firoozkuh sand. This silt is non-plastic and its plasticity index (PI) cannot be discerned. Optical images of Firoozkuh sand and silt grains are shown in Fig. 1. Also, chemical composition analysis by X-ray fluorescence (XRF) test was performed on both Firoozkuh sand and silt (ASTM E 1621) and the results are presented in Table 1. The results indicate that the major part of both soils consists of silica (SiO_2) in the form of quartz. The sand was mixed with the appropriate amount of silt to produce a sand–silt mixture with 0, 10, 20, 30, 50, 70 and, 100 percent fines content. The physical properties of sand–silt mixtures and their nomenclature are presented in Table 2. Also, the grain size distribution is exhibited in Fig. 2.

In this study, the minimum void ratio (e_{min}) for each sand–silt mixture was determined using the vibratory table method (ASTM D4253) and also the modified proctor compaction method (ASTM D1557) for all range of fines content. As shown in Fig. 3, both

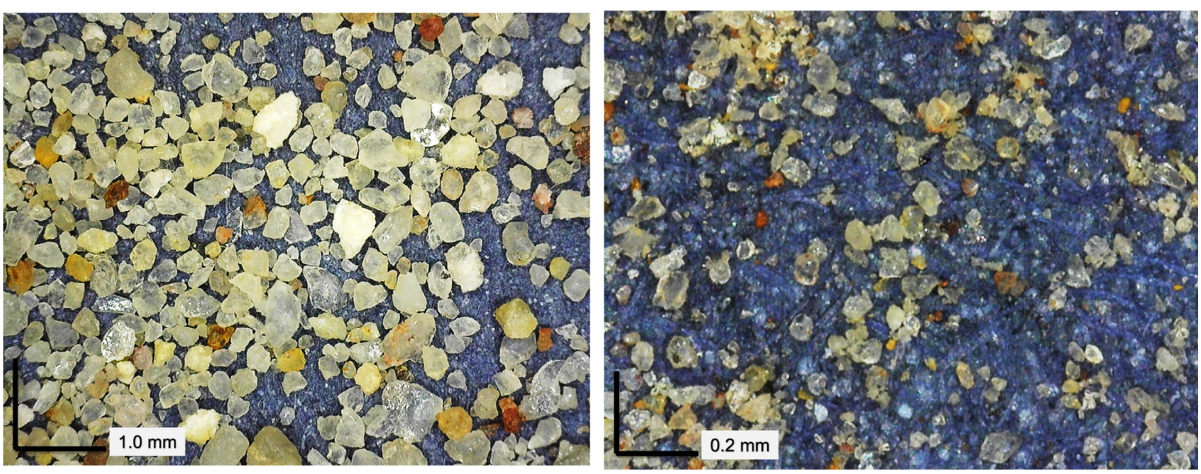

(a) Firoozkuh Sand (b) Firoozkuh silt

Fig. 1 Optical images of soil grains **a** Firoozkuh sand; and **b** Firoozkuh silt

Table 1 Soils chemical composition by XRF analysis

Oxide composition (%)	SiO_2	Al_2O_3	Fe_2O_3	K_2O	CaO	TiO_2	Na_2O	MgO	P_2O_5	SO_3	LOI
Firoozkuh sand	92.57	2.16	2.66	0.21	1.44	0.22	>>	>>	>>	>>	0.70
Firoozkuh silt	89.93	3.15	3.25	0.22	1.08	1.01	>>	>>	>>	–	1.31

Table 2 Physical properties and nomenclature of sand–silt mixtures used in the present study

Soil type	Soil name	D_{50}	C_u	C_c	G_s	e_{max}	e_{min}
Firoozkuh Sand	FS0	0.3	1.92	0.93	2.641	0.926	0.620
Sand + 10%Silt	FS10	0.29	4.46	2.17	2.644	0.826	0.513
Sand + 20%Silt	FS20	0.28	6.98	2.53	2.648	0.735	0.457
Sand + 30%Silt	FS30	0.245	8.28	0.55	2.652	0.693	0.409
Sand + 50%Silt	FS50	0.075	7.5	0.44	2.656	0.809	0.418
Sand + 70%Silt	FS70	0.055	2.5	1.17	2.660	0.947	0.507
Firoozkuh Silt	FS100	0.046	2.43	1.14	2.678	1.208	0.644

C_u Uniformity coefficient; C_c Curvature coefficient; and G_s Specific gravity

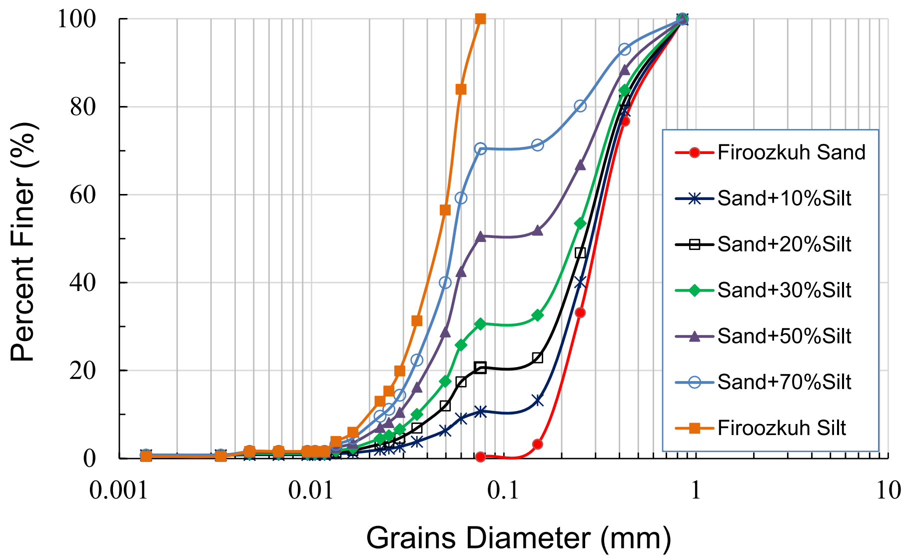

Fig. 2 Grain size distribution of the sand–silt mixtures used in present study

methods yielded the same results for fines content between 0 and 30%, but their results deviated when fines content increased from 30 to 100%. As vibratory table is explicitly recommended for fines contents less than 15%, the results of modified proctor compaction method were used for the determination of e_{min} of sand–silt mixture with fines contents greater than 30%.

The ASTM D4254 standard was used to determine the maximum void ratio (e_{max}) for sand–silt mixtures. Although the standard has recommended this procedure for fines contents less than 15%, both methods A and C of this standard were employed for the entire range of fines contents. In Method A, the soil was placed as loosely as possible into the mold by pouring continuous flow of soil from a spout. However, to prevent issues such as spout clogging and soil particle segregation for mixtures with fines content greater than 20%, a scoop, rather than the spout, was employed. In Method C, 1000 g of soil were poured into a 2000-mL graduated cylinder, and a stopper was securely placed at the top of the cylinder. The cylinder was then inverted upside down and promptly returned to its original upright position, facilitating the pluviation of soil into a loose arrangement. As shown in Fig. 3, both methods exhibit almost the same results. Since method A usually produces more accurate and repeatable results, its results were used for the determination of e_{max} in this study.

As illustrated in Fig. 3, the e_{max} and e_{min} decrease to a minimum value with increasing the fines content until fines content reaches a threshold value (in this case around 30%), and then, they both increase with further increase in the fines content up to 100%, which is in agreement with the previous research (e.g., Polito 1999; Hazirbaba and Rathje 2009; Yazdani et al. 2022). This threshold value, identified as a turning point in both e_{max} and e_{min} diagrams, is

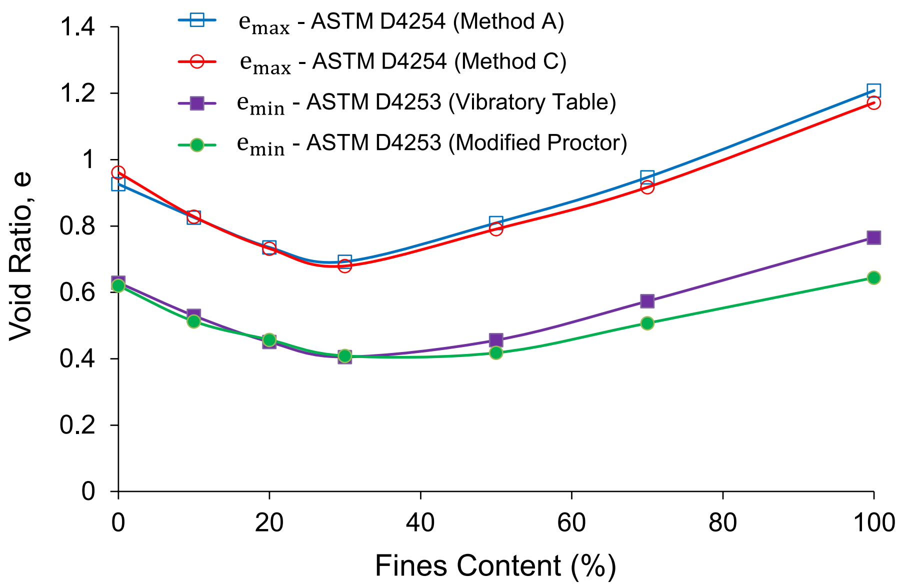

Fig. 3 Minimum and maximum void ratio Vs fines content for Firoozkuh sand–silt mixtures

the maximum amount of fines content that can be placed in the void spaces between coarse grains without any change in the volume of the coarse grains matrix. The threshold fines content is a transition point in which the soil microstructure changes from "fines in a coarse matrix" to "coarse grains in the fines matrix" (Rahman et al. 2008).

2.2 Test Procedure

A series of 35 strain-controlled cyclic triaxial tests were performed using a servo-controlled hydraulic cyclic triaxial apparatus at Geotechnical Research Center (GRC) of Iran University of Science and Technology (IUST). Specimens were 50 mm in diameter and 101 mm in height and were prepared by moist tamping at a specified water content value, using the under-compaction method (Ladd 1978). The moist tamping technique was preferred in this study since it could produce specimens with low relative densities (Ishihara 1993) and also avoided the segregation of sand and silt particles (Yang et al. 2006).

Carbon dioxide (CO_2) was percolated through the specimens to remove the air from the soil pores (40 min with 1 kPa for clean sand and 90 min with 3 kPa for silty sand specimens) and then, de-aired water was slowly circulated through the specimens from bottom to top to saturate the specimen.

For achieving full saturation, cell pressure (initial value of 20 kPa) and backpressure were simultaneously increased to the final backpressure of 140 kPa for all specimens. This value was found to be the minimum value needed to gain Skempton B-values greater than 0.95 for specimens with high fines content. Afterward, specimens were isotropically consolidated up to the desired effective confining stress. Finally, strain-controlled cyclic loading was applied to the specimens under the undrained condition with 0.1 Hz frequency.

Due to the isotropic consolidation and strain-controlled condition, the onset of liquefaction was considered when EPWP reached the initial effective confining stress (i.e., zero effective stress) for all tests. Table 3 presents the characteristics of performed tests.

3 Cyclic Tests Databank for Model Development

To present a more generalized EPWP model, a number of undrained cyclic tests,performed on clean sand and silty sand containing nonplastic silt, were collected from previous studies. These tests results were reanalyzed and desired data were calculated for the aim of present study.

Arulmoli et al. (1992), performed several cyclic simple shear and cyclic triaxial tests on Nevada sand for the VELACS program. The Nevada sand

Table 3 Summary of tests performed in the present study

No	Test ID	Fine content (%)	Dr (%)*	σ'_m (kPa)	Strain amplitude (%)	Skempton B-value (%)	W_{liq} (J/m^3)
1	F0D20S50	0	19.1	50	0.2	> 97	560
2	F0D20S100	0	19.8	100	0.25	> 97	1070
3	F0D20S200	0	23.3	200	0.25	> 96.5	3690
4	F0D40S50	0	42.8	50	0.25	> 96.5	1500
5	F0D40S100	0	41.5	100	0.2	> 96.9	2850
6	F0D40S200	0	39.7	200	0.35	> 96.1	5290
7	F0D60S50	0	58.0	50	0.25	> 96	3480
8	F0D60S100	0	62.2	100	0.3	> 96	10,060
9	F0D60S200	0	60.8	200	0.35	> 96	13,250
10	F0D80S50	0	78.2	50	0.3	> 96.3	6050
11	F0D80S100	0	81.9	100	0.35	> 97	19,150
12	F10D20S100	10	20.2	100	0.2	> 97	3400
13	F10D40S100	10	41.3	100	0.25	> 96.6	5380
14	F10D60S100	10	59.8	100	0.3	> 96	13,800
15	F10D80S100	10	81.1	100	0.35	> 96.6	26,000
16	F10D100S200	10	98.8	200	0.35	> 97.1	90,100
17	F20D20S100	20	19.7	100	0.2	> 96.8	1610
18	F20D40S100	20	41.4	100	0.25	> 96.5	3780
19	F20D60S100	20	61.7	100	0.3	> 96.6	6950
20	F20D80S100	20	79.0	100	0.35	> 96	13,150
21	F30D20S100	30	19.1	100	0.2	> 97.1	450
22	F30D40S50	30	40.3	50	0.2	> 96.7	480
23	F30D40S100	30	41.9	100	0.25	> 97	900
24	F30D40S200	30	42.5	200	0.3	> 96	2050
25	F30D60S100	30	62.7	100	0.3	> 96.7	3390
26	F30D60S200	30	58.8	200	0.35	> 98.4	6230
27	F30D80S100	30	79.0	100	0.35	> 96	9790
28	F50D40S100	50	40.2	100	0.25	> 96.6	535
29	F50D60S100	50	62.0	100	0.3	> 96	2380
30	F70D40S100	70	41.2	100	0.25	> 97.2	520
31	F70D60S100	70	63.8	100	0.25	> 96.6	2580
32	F100D20S100	100	24.1	100	0.15	> 96.9	515
33	F100D40S100	100	43.0	100	0.2	> 96.2	725
34	F100D60S100	100	61.8	100	0.25	> 97.6	2280
35	F100D80S100	100	81.8	100	0.35	> 96.7	13,100

*Relative density after consolidation

properties are listed in Table 4. The specimens were prepared by the dry pluviation method and the tests were performed using undrained stress-controlled cyclic loading with a frequency of approximately 1 Hz. Despite two different stress–strain paths in cyclic simple shear and cyclic triaxial tests, the results of the energy method were compatible with each other as anticipated. The brief information of these 15 tests is presented in Table 5.

Liang (1995), performed several cyclic torsional shear tests on Reid Bedford sand and Lower San Fernando Dam (LSFD) sand using a hollow cylinder apparatus. The properties of both types of sands are listed in Table 4. The specimens were prepared using the dry deposition method in 6 layers. Then two types

Table 4 Physical properties of soils tested in previous studies collected for database

Soil name	Fine content (%)	D_{50} (mm)	C_u	C_c	G_s	e_{max}	e_{min}
Nevada sand	7.7	0.15	2.27	0.95	2.67	0.887	0.511
Reid Bedford sand	0	0.26	1.8	1	2.65	0.85	0.58
LSFD	28	0.13	4.35	1.8	2.67	1.22	0.71

Table 5 Summary of tests performed in the previous studies collected for database

No	Test ID	soil name	Dr (%)	σ'_m(kPa)	Test type	Loading type (amplitude)	W_{liq} (J/m^3)
36	CSS4006	Nevada sand	42.6	160	CSS	CSR(0.134)	1469
37	CSS4007	Nevada sand	43.3	160	CSS	CSR(0.071)	1253
38	CSS4008	Nevada sand	44.9	80	CSS	CSR(0.181)	834
39	CSS4009	Nevada sand	45.9	80	CSS	CSR(0.092)	644
40	CSS6004	Nevada sand	63	80	CSS	CSR(0.295)	1525
41	CSS6005	Nevada sand	62.7	80	CSS	CSR(0.155)	1367
42	CSS6006	Nevada sand	61.4	160	CSS	CSR(0.163)	1961
43	CSS6007	Nevada sand	60.1	160	CSS	CSR(0.084)	2136
44	CSS6008	Nevada sand	61.7	160	CSS	CSR(0.164)	2277
45	CY40114	Nevada sand	42.4	80	CT	CSR(0.18)	1022
46	CY40115	Nevada sand	41.6	40	CT	CSR(0.232)	398
47	CY40116	Nevada sand	42.3	160	CT	CSR(0.152)	2887
48	CY6086	Nevada sand	61.6	80	CT	CSR(0.5)	1058
49	CY6087	Nevada sand	61.6	80	CT	CSR(0.75)	1559
50	CY6088	Nevada sand	60.6	40	CT	CSR(0.61)	603
51	RBLHL	Reid Bedford sand	52.9	124.4	HTST	Strain(0.15%)	1503
52	RBLHM	Reid Bedford sand	49.7	124.1	HTST	Strain(0.47%)	1496
53	RBMLL	Reid Bedford sand	59.1	41.4	HTST	Strain(0.15%)	738
54	RBMML	Reid Bedford sand	61.1	82.7	HTST	Strain(0.15%)	1338
55	RBMMM	Reid Bedford sand	59.3	82.7	HTST	Strain(0.47%)	1317
56	RBMMH1	Reid Bedford sand	61.2	82.7	HTST	Strain(1.02%)	1303
57	RBMHL	Reid Bedford sand	59.5	124.1	HTST	Strain(0.15%)	1813
58	RBMHM	Reid Bedford sand	63.8	124.1	HTST	Strain(0.47%)	1758
59	RBHHL	Reid Bedford sand	68.8	124.1	HTST	Strain(0.15%)	2303
60	RBHHM	Reid Bedford sand	72.6	124.1	HTST	Strain(0.47%)	2386
61	RBHHH	Reid Bedford sand	70.9	124.1	HTST	Strain(1.02%)	2737
62	RBLMR	Reid Bedford sand	54.9	82.7	HTST	Random	1150
63	RBMLR	Reid Bedford sand	57.5	41.4	HTST	Random	851
64	RBMMR	Reid Bedford sand	58.3	82.7	HTST	Random	1538
65	RBMHR	Reid Bedford sand	59.9	124.1	HTST	Random	1943
66	RBHMR	Reid Bedford sand	67.5	82.7	HTST	Random	1955
67	Test102, LSFD_LLR	LSFD	57.2	41.4	HTST	Random	517
68	Test105, LSFD_LMR	LSFD	60	82.7	HTST	Random	797
69	Test114, LSFD_LMR	LSFD	59.9	82.7	HTST	Random	802
70	Test115, LSFD_LHR	LSFD	61.1	124.1	HTST	Random	1294
71	Test113, LSFD_HMR	LSFD	79.2	82.7	HTST	Random	811
72	Test120, LSFD_HMR	LSFD	87.4	82.7	HTST	Random	827

CSS cyclic simple shear test, *CT* cyclic triaxial test, *HTST* hollow torsional shear test of loading including strain-controlled loading (with three levels of strain amplitudes and frequency of 0.1 Hz), and random loading (in order to simulate the loading of an earthquake) were applied to the specimens. Table 5 also shows the information of these 22 tests.

Finally, using these 37 collected test results along with the results of 35 tests performed in the present study, the database consists of 72 cyclic tests which the distribution of relative density (19.1–98.8%), fines content (0–100%), and effective confining stress (40–200 kPa) of specimens are presented in Table 6.

4 Tests Results and Analyses

The dissipated energy per unit volume of soils (W) was computed by Eq. (1) which σ_{ij} and $d\varepsilon_{ij}$ are stress and incremental strain tensors, respectively (Green 2001).

$$W = \int dW = \int \sigma_{ij} d\varepsilon_{ij} \tag{1}$$

By applying the terms of saturated state, undrained loading and boundary conditions to Eqs. (1), (2) for cyclic triaxial tests, and Eq. (3) for cyclic torsional shear and cyclic simple shear tests are derived. In the Eq. (2), $\sigma_{d,i}$, $\varepsilon_{a,i}$, and n are the ith increment in deviatoric stress, ith increment in axial strain, and the total number of increments, respectively. Similarly, in Eq. (3), τ_i, γ_i, and n are the ith increment in shear stress, the ith increment in shear strain, and the total number of increments, respectively.

$$W = \frac{1}{2}\sum_{i=1}^{n-1}(\sigma_{d,i+1} + \sigma_{d,i})(\varepsilon_{a,i+1} - \varepsilon_{a,i}) \tag{2}$$

$$W = \frac{1}{2}\sum_{i=1}^{n-1}(\tau_{i+1} + \tau_i)(\gamma_{i+1} - \gamma_i) \tag{3}$$

As a typical result of the strain-controlled cyclic triaxial tests performed for the present study, Fig. 4a–d represents the results of test No. 3 (F0D20S200) of Table 3. Applied cyclic axial strain (0.25%), cyclic deviatoric stress, excess pore water

Table 6 Distribution of relative density, fines content and effective confining stress of tests in database used for EPWP model development

Relative density (%)	Num. of tests	Fines content (%)	Num. of tests	σ'_m(kPa)	Num. of tests
0–5	0	0–5	27	0–10	0
5–10	0	5–10	15	10–20	0
10–15	0	10–15	5	20–30	0
15–20	4	15–20	0	30–40	0
20–25	3	20–25	4	40–50	5
25–30	0	25–30	6	50–60	5
30–35	0	30–35	7	60–70	0
35–40	1	35–40	0	70–80	0
40–45	16	40–45	0	80–90	17
45–50	2	45–50	0	90–100	0
50–55	2	50–55	2	100–110	24
55–60	11	55–60	0	110–120	0
60–65	20	60–65	0	120–130	9
65–70	2	65–70	0	130–140	0
70–75	2	70–75	2	140–150	0
75–80	4	75–80	0	150–160	0
80–85	3	80–85	0	160–170	6
85–90	1	85–90	0	170–180	0
90–95	0	90–95	0	180–190	0
95–100	1	95–100	4	190–200	6

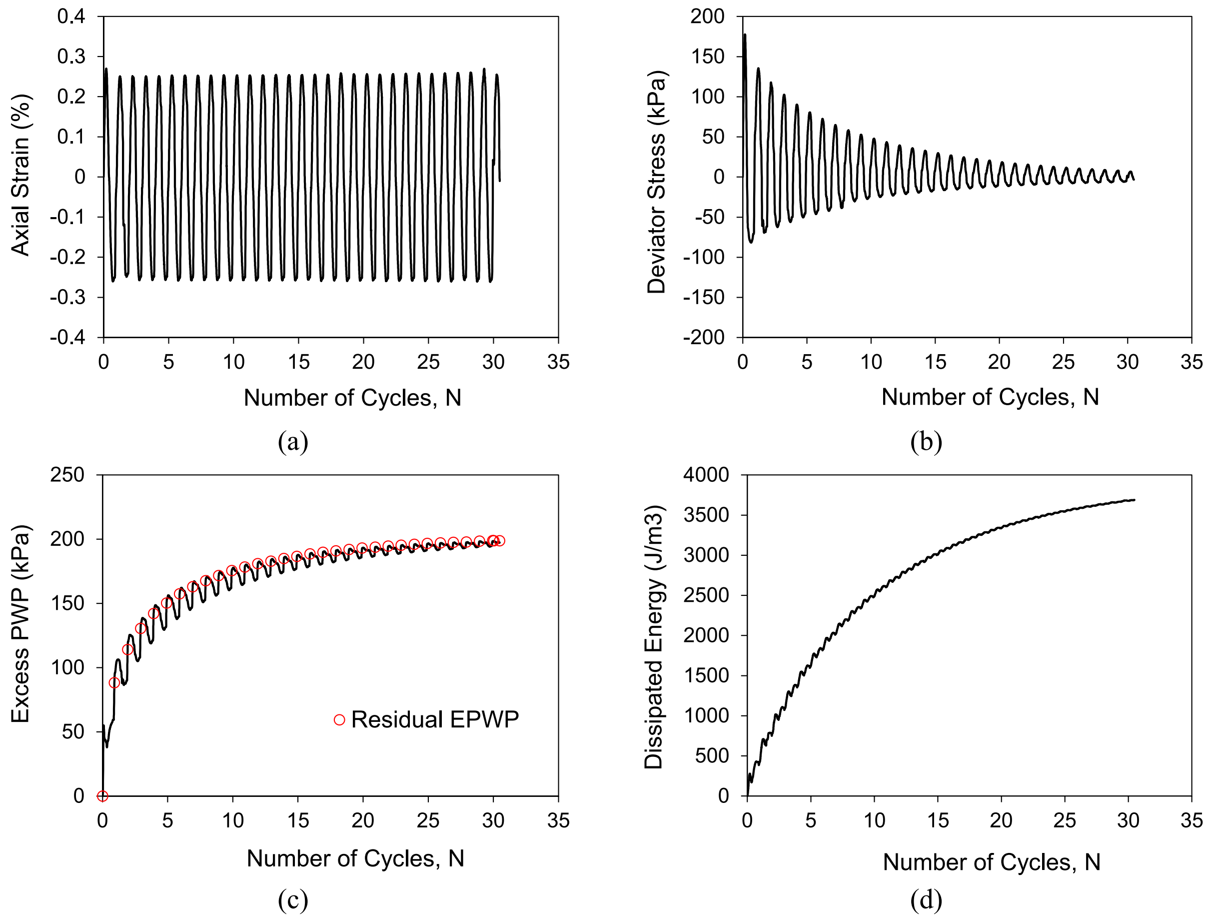

Fig. 4 Time history of **a** cyclic axial strain, **b** cyclic deviator stress, **c** excess pore water pressure, and **d** dissipated energy for Firoozkuh sand at $D_r = 23.3\%$ and $\sigma'_m = 200\,\text{kPa}$

pressure, and dissipated energy versus cycle number are shown in Fig. 4a–d, respectively.

In this test, the corresponding deviatoric stress has a maximum value at the beginning of the cyclic loading (175 kPa) and tends to decrease as cyclic loading continues and eventually reaches a residual value (6 kPa) while the shear-induced excess pore water pressure increases gradually and reaches the initial effective confining stress (i.e., the onset of liquefaction). As shown in Fig. 4c, during cycles of loading, excess pore water pressure fluctuates, but the amounts of residual EPWP are assigned as representative of the entire EPWP history. Residual EPWPs are the results of plastic deformation in soil skeleton and are assumed to be those at the time when the applied cyclic stress (e.g. deviator stress in the triaxial test or shear stress in the simple shear test) equals or crosses zero (Dobry et al. 1982; Green et al. 2000). The residual EPWPs are depicted in Fig. 4c by red circles. As cyclic loading continues, cumulative dissipated energy (W) increases until reaches the capacity energy (W_{liq}) (Fig. 4d). Moreover, the axial stress–strain hysteresis loops and stress path diagram of this test are illustrated in Fig. 5a and b, respectively.

Figure 6a–d shows the difference in the trend of energy dissipation for strain-controlled and stress-controlled tests. In test No. 3 of Table 3 (as a strain-controlled test), the specimen has been liquefied after 32 cycles (W_{liq}=3690 J/m^3). As shown in Fig. 6a, the greatest amount of energy dissipation occurs in the first cycle (473 J/m^3) and as loading continues, the energy dissipation of each cycle decreases. The last cycle has the lowest amount of energy dissipation (22

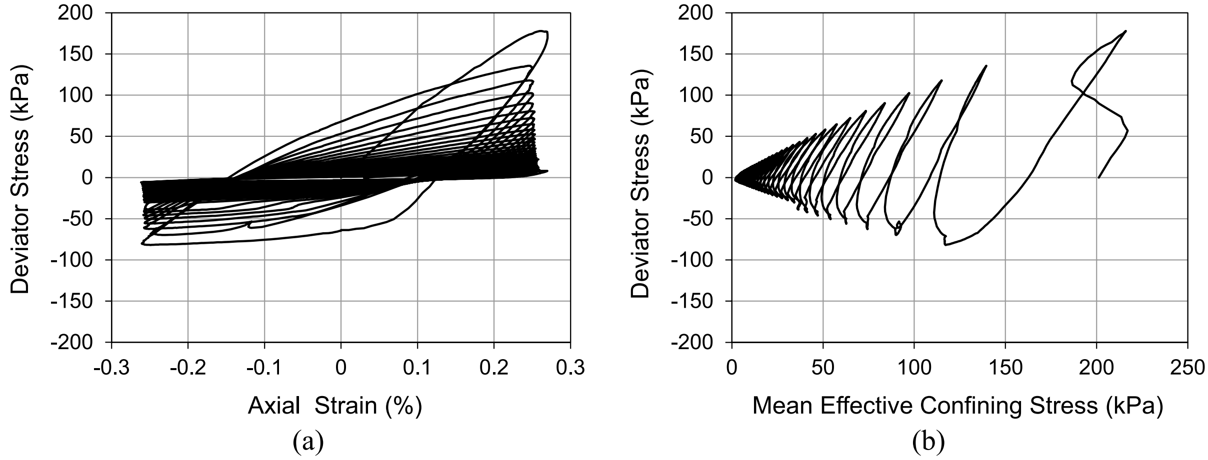

Fig. 5 **a** axial stress–strain hysteresis loops, and **b** stress path for undrained cyclic triaxial test on Firoozkuh sand at $D_r = 23.3\%$ and $\sigma'_m = 200\text{kPa}$

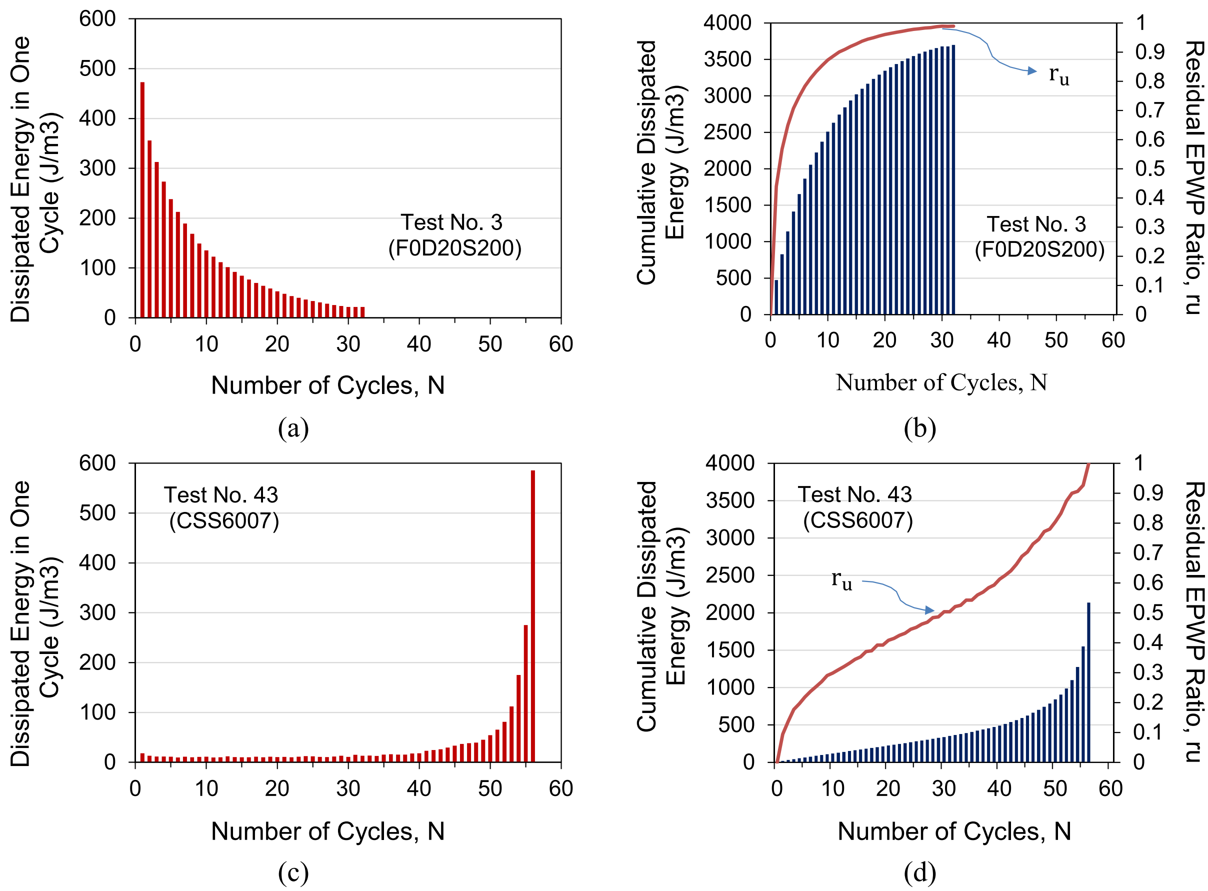

Fig. 6 Histogram of **a** dissipated energy in each cycle, and **b** cumulative dissipated energy for test No. 3 (F0D20S200), **c** dissipated energy in each cycle, and **d** cumulative dissipated energy for test No. 43 (CSS6007)

J/m^3). Also, the half of energy dissipation, required for the onset of liquefaction, occurs at the first 6 cycles (Fig. 6b). In test No. 43 of Table 5 (as a stress-controlled test), the specimen has been liquefied after 56 cycles (W_{liq}= 2136 J/m^3). As shown in Fig. 6c, the first cycle has the lowest amount of dissipated energy (18 J/m^3) and as loading continues, the energy dissipation of each cycle increases such that the greatest amount of energy dissipation (almost 30% of W_{liq}) occurs at the last cycle.

The difference in the above behavior is related to the type of loading. In the strain-controlled cyclic loading test, the major part of energy dissipation and EPWP increase occurs in the first loops. Also, since the applied strain is controlled in this test, the specimen preserves its shape and does not undergo sudden failure. Conversely, in the stress-controlled cyclic loading test, as loading continues, the EPWP increases and soil stiffness is degraded, and its strain increases. So, the major part of energy dissipation and EPWP increase occurs in the last few loops and determination of the exact moment of the onset of liquefaction may be difficult. In fact, a slight mistake in the determination of the cycle reaching the onset of liquefaction may lead to a significant inaccuracy in liquefaction capacity. Also, the extreme deformation of the specimen occurs near the onset of liquefaction which may introduce errors in the calculation of capacity energy.

As presented in tests 54–56 of Table 5, three strain-controlled tests were performed on the Reid Bedford sand with the same initial condition (D_r = 60% and σ'_m = 82.7 kPa) and with three different strain amplitudes of 0.15, 0.47, and 1.02% resulted in capacity energy of 1338, 1317, and 1303 (j/m^3), respectively.

Similarly, as presented in tests 40, 41, 48, and 49 of Table 5, four stress-controlled tests were performed on Nevada sand with the same initial condition (D_r = 60% and σ'_m = 80 kPa) and with four different CSR of 0.295, 0.155, 0.5, and 0.75 resulted in capacity energy of 1525, 1367, 1058, and 1559 (j/m^3), respectively. Comparing the results of these two tests series indicates that the strain-controlled tests can determine the capacity energy more accurate than the stress-controlled tests. So, all the tests performed in the present study were conducted in strain-controlled mode.

The results of all performed and collected tests are analyzed and residual EPWP versus dissipated energy (W) of each test is elicited to create a dataset for statistical analysis.

5 EPWP Model Development

The residual EPWP is usually presented in terms of residual EPWP ratio (r_u). The residual EPWP ratio (r_u) is defined as the ratio of the residual EPWP to the initial effective confining stress. Several energy-based residual EPWP ratio models were proposed using cyclic test results by previous researchers. The model proposed by Polito et al. (2008), presented in Eq. (4), is the only available energy-based EPWP model which takes into account the effect of fines content as a key parameter.

$$r_u = \sqrt{\frac{W_s}{PEC}} \leq 1 \tag{4}$$

where W_s is energy dissipated per unit volume of soil divided by the initial effective confining stress, and PEC is a calibration parameter, named "pseudoenergy capacity". Polito et al. (2008) presented Eq. (5) for PEC.

$$\ln(PEC) = \begin{cases} \exp\left(0.0139 \cdot D_r\right) - 1.021, & FC < 35\% \\ \exp\left(0.0139 \cdot D_r\right) - 1.021 - 0.597 \cdot FC^{0.312}, & FC \geq 35\% \end{cases} \tag{5}$$

Based on a series of cyclic hollow cylinder torsional shear tests on Toyoura sand, Jafarian et al. (2012) proposed Eq. (6) for r_u of clean sands.

$$r_u = \left(\frac{\alpha^{W/W_{liq}} - 1}{\alpha - 1}\right)^{0.845} \tag{6}$$

where α is correlation parameter and determined as:

$$\alpha = 0.5052 - 0.593(D_r/100) \tag{7}$$

Among these models, the authors find that the model proposed by Jafarian et al. (2012) has a more suitable functional form. However, this model originally was developed based on tests performed on clean sand and it cannot properly predict the EPWP generation in sand–silt mixtures. A simple model has been used in the present study, as given in Eq. (8). In this model, C is calibration parameter and W_{liq} is the capacity energy of soil. Also, W is the cumulative dissipated energy at a given time of loading. A great feature of this model is that the dissipated energy (W) is normalized by the capacity energy of the soil (W_{liq}), and by this means, the effect of W_{liq} (and other parameters which W_{liq} depends on them) on the model can be excluded.

$$r_u = \sqrt{\frac{1 - C^{W/W_{liq}}}{1 - C}} \tag{8}$$

The results of residual EPWP versus dissipated energy (W) for tests F0D20S50 (FC=0%, D_r=20% and $\sigma'_0 = 50$ kPa), F0D20S100 (FC=0%, D_r=20% and $\sigma'_0 = 100$ kPa) and F0D20S200 (FC=0%, D_r=20% and $\sigma'_0 = 200$ kPa) are plotted in Fig. 7a. As shown in Fig. 7b, when these results are re-plotted in terms of $r_u - W/W_{liq}$ (excess pore water pressure normalized by initial effective confining stress versus dissipated energy normalized by capacity energy), they yield in almost the same shape. So, it is inferred that the $r_u - W/W_{liq}$ relationship is independent of initial effective confining stress, as previously stated by Jafarian et al. (2012). Also, further statistical study of other test results of the database confirmed that initial effective confining stress had a negligible effect on the model calibration parameter.

Similarly, the results of residual EPWP versus dissipated energy (W) for tests F0D20S100 (FC=0%, D_r=20% and $\sigma'_0 = 100$ kPa), F0D40S100 (FC=0%, D_r=40% and $\sigma'_0 = 100$ kPa), F0D60S100 (FC=0%, D_r=60% and $\sigma'_0 = 100$ kPa), and F0D80S100 (FC=0%, D_r=80% and $\sigma'_0 = 100$ kPa) are plotted in Fig. 8a. As shown in Fig. 8b, when the results are re-plotted in terms of $r_u - W/W_{liq}$, the data fall within a narrow band and the curvature of $r_u - W/W_{liq}$ curve increases with increasing of relative density. So, it can be inferred that the $r_u - W/W_{liq}$ relationship is dependent on the relative density.

The nonlinear regression analysis was used for the determination of model calibration parameter (i.e., C). The parameter C controls the curvature of the model and can be determined by Eq. (9).

$$C = a - b \cdot \left(D_r/100\right) \tag{9}$$

where D_r is relative density in percent and a and b are the model coefficients, with the b equal to 0.441 and a is dependent on fines content. The a is determined for each subgroup of data with the same fines content and its variation versus fines content is plotted in Fig. 9. As may be observed from this figure, the coefficient a increases with increasing fines content until the fines content reaches a threshold value and then, the

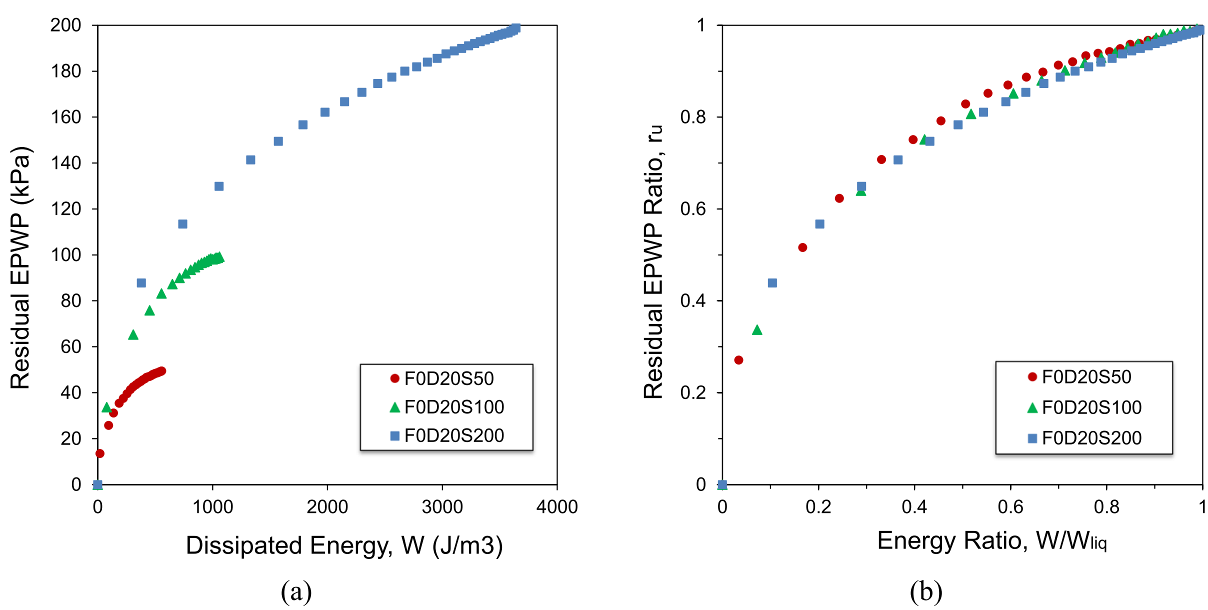

Fig. 7 Comparing results of test No. 1 (F0D20S50), test No. 2 (F0D20S100), and test No. 3 (F0D20S200) in terms of **a** residual excess pore water pressure versus dissipated energy, and **b** residual excess pore water pressure ratio versus energy ratio

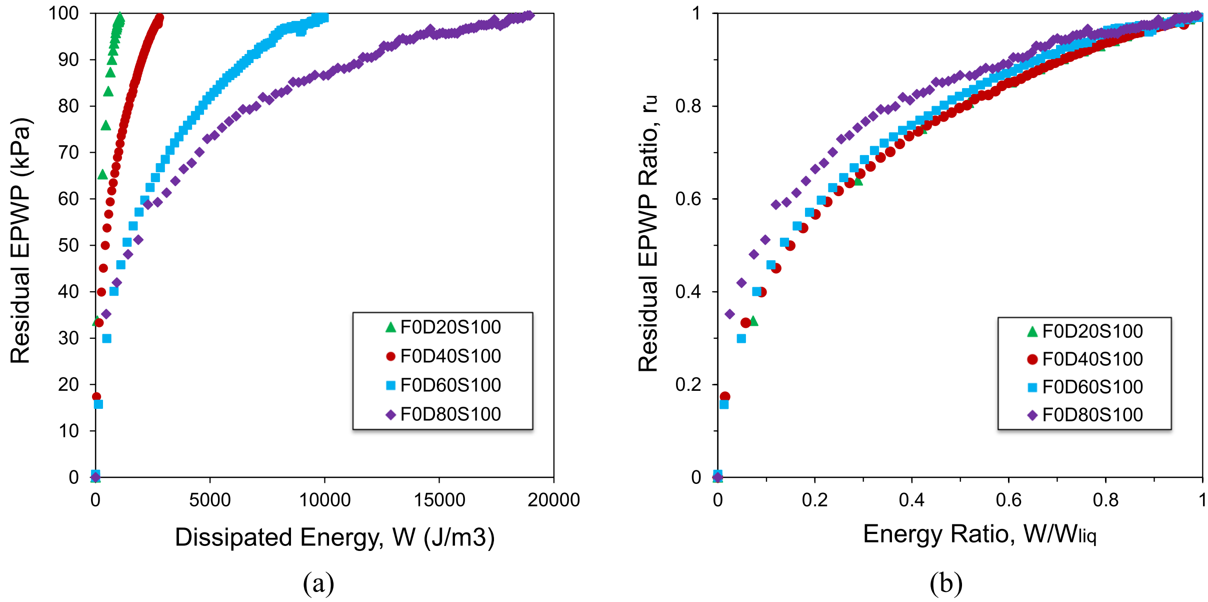

Fig. 8 Comparing results of test No. 2 (F0D20S100), test No. 5 (F0D40S100), test No. 8 (F0D60S100) and test No. 11 (F0D80S100) in terms of **a** residual excess pore water pressure versus dissipated energy, and **b** residual excess pore water pressure ratio versus energy ratio

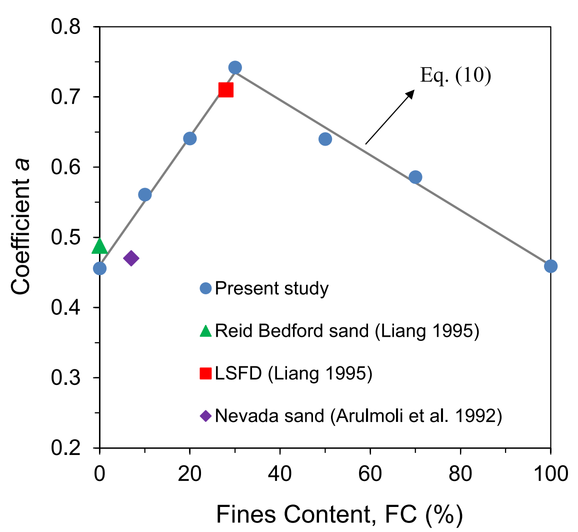

Fig. 9 Variation of coefficient *a* versus fines content

a decreases with further increase in fines content from this threshold value up to 100% (i.e., pure silt). Logically, the variation trend of coefficient *a* is consistent with the threshold fines content concept (previously mentioned). Also, the value of coefficient *a* is almost identical for clean sand and pure silt. The coefficient *a* can properly be estimated by Eq. (10).

$$a = \begin{cases} 0.46 + 0.9167 \cdot (FC/100) & if \quad FC \leq 30\% \\ 0.8529 - 0.3929 \cdot (FC/100) & if \quad FC > 30\% \end{cases} \tag{10}$$

The used database in this study consist of 72 cyclic tests and the number of data points in each test is equal to the number of load cycles till the onset of liquefaction (N_l). Therefore, a test with more load cycles (i.e., more data points) can have more influence on the determination of model coefficients than a test with fewer ones. In order to avoid such an effect, data points of each test were weighted by a factor of $1/N_l$ and So, each test produces the same number of data points as other tests.

R^2 (coefficient of determination), MAE (mean absolute error), and the σ (standard deviation) of the residuals ($r_{u,measured} - r_{u,predicted}$) of Eq. (8) are 0.95, 0.0417, and 0.06 respectively. Also, the mean of residuals of Eq. (8) for each subgroup of data points with the same effective confining stress are plotted in Fig. 10, which shows that the residuals are not biased due to effective confining stress.

For demonstration of the models' performance, the measured and predicted values of residual EPWP ratio for six individual tests are shown in Fig. 11. As

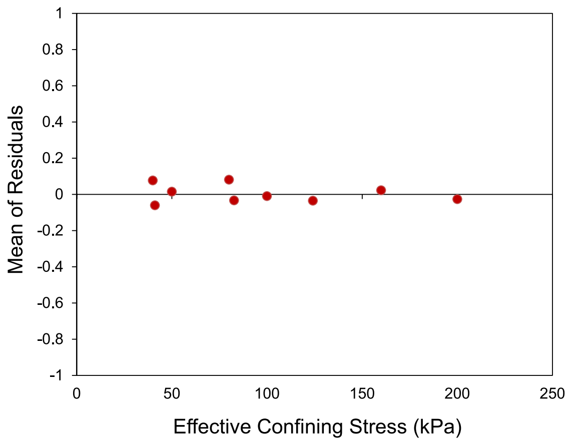

Fig. 10 Mean of residuals of the presented model versus effective confining stress

shown in this figure, the model presented by Polito et al. (2008) cannot correctly predict r_u values. The reason for this poor performance is that Eq. (5) (i.e., PEC): (1) does not consider the effect of FC on r_u of mixtures with FC<35%, and (2) cannot accurately predict PEC values for different soils. The model presented by Jafarian et al. (2012) produces relatively acceptable results; however, it usually underestimates r_u values. Convincingly, the model proposed in the present study can properly predict r_u values.

In the proposed model, both abscissa (W/W_{liq}) and ordinate (r_u) vary between 0 and 1 and the calibration parameter C controls the curvature of the $r_u - W/W_{liq}$ curve. As shown by the results, this model can estimate r_u values very well, but it must be noticed that the accuracy of the model strongly depends on the accuracy of determination of the capacity energy (W_{liq}). In practice, the capacity energy (W_{liq}) of any soil under consideration can be either directly determined by cyclic tests in the lab or estimated by proposed correlations (e.g., Dief and Figueroa 2007; Jafarian et al. 2012; Yang and Pan 2018; Sonmezer 2019; Ghorbani and Eslami 2021; Kanth et al. 2024).

It should be noted, although, different sample preparation techniques (moist tamping, dry deposition, and dry pluviation) were used in cyclic tests of the compiled database, the results were compatible and trends were consistent regardless of sample preparation techniques (Fig. 9).

The proposed model can directly relate the factor of safety (FS), defined by the ratio of capacity energy to demand energy (i.e., W_{liq}/W), to r_u and this is a great advantage of the model. It is noticeable that the values of FS in the EMB and the SMB are not comparable in quantity, and same r_u could be related to different values of FS in different methods.

6 Validation of Proposed EPWP Model

The proposed EPWP model, developed based on a database consisting of 72 cyclic tests performed on specimens with various soil types and wide ranges of fines content, initial effective confining stress, relative density, and different loading path, was verified using three physical modeling centrifuge tests, and the field case history, recorded at Wildlife downhole array site during 1987 Superstition Hills earthquake.

6.1 Centrifuge Tests

Dief (2000) conducted a series of centrifuge tests on the Nevada, Reid Bedford, and Lower San Fernando Dam sands (the same soils previously used by Liang (1995) and Arulmoli et al. (1992), described in Sect. 3). The centrifuge tests were conducted in a laminar box to simulate the response of level ground sites to dynamic loading. Figure 12 illustrates schematically the laminar box, model configuration, and instrumentation included in the soil (Dief and Figueroa 2007). The recorded accelerations and displacements at different depths within the soil layers were used to calculate the shear stress–strain time histories and the dissipated energy at any instance of time. The details of these tests can be found in Dief (2000).

The first test, N60H, was conducted on the Nevada sand with a relative density of 58.5%, representing a prototype depth of 7.6 m. The dissipated energy time history at depth of 3.39 m was estimated using recorded acceleration at depth of 3.42 m (AH2) and 1.86 m (AH3). Then, this dissipated energy time history in conjunction with recorded pore water pressure at depth of 3.39 m (P2) was used to produce $r_u - W/W_{liq}$ diagram at depth of 3.39 m, illustrated in Fig. 13. The capacity energy (W_{liq}) was determined from the dissipated energy time history when the recorded pore pressure ratio (r_u) reached one. This capacity energy (W_{liq}) along with relative density (D_r=58.5%) and fines content (FC=8%), as input parameters, were set into the proposed EPWP model and the Predicted values are demonstrated in Fig. 13. According to this figure, there is an acceptable agreement between measured and predicted pore pressure ratio in centrifuge condition. It is noticeable that this model, as other similar EPWP models, inherently predicts the residual EPWP ratio and cannot consider the fluctuations of transient EPWP ratio due to the changes in mean normal stresses applied by seismic loadings (Green et al. 2000).

The second test, LSF50H, was conducted on the Lower San Fernando Dam sands with a relative density of 62.8%, representing a prototype depth of 7.6m. The dissipated energy time history at depth of 3.18 m was estimated using recorded acceleration at depth of 3.22 m (AH2) and 1.74 m (AH3). Then, this dissipated energy time history in conjunction with recorded pore water pressure at depth of 3.18 m (P2) was used to produce $r_u - W/W_{liq}$ diagram at depth of 3.18 m, illustrated in Fig. 14. The determined capacity energy (W_{liq}) along with relative density ($D_r = 62.8\%$) and fines content ($FC = 28\%$), as input parameters, were set into the proposed EPWP model and the Predicted values are demonstrated in Fig. 14. As shown in this figure, the model slightly overestimates r_u values, but differences between predicted and measured r_u values at the end of load cycles (peak values) are not significant and less than 0.05.

The third test, RB60L, was conducted on the Reid Bedford sand with a relative density of 60.5%, representing a prototype depth of 5.7 m. The $r_u - W/W_{liq}$ diagram at the depth of 2.75 m are plotted in Fig. 15 using recorded acceleration at depths of 2.87 m (AH2) and 1.72 m (AH3) in conjunction with recorded pore water pressure at the depth of 2.75 m (P2). According to this figure, the proposed EPWP model can accurately predict r_u values.

6.2 Wildlife Downhole Array Site Data

The Wildlife site is located on the west side of the Alamo River in Imperial Wildlife Management Area (Imperial County, California). The geotechnical investigations showed that the site consists of a very loose silt layer between 0 to 2.5 m depth, a loose silty sand layer between 2.5 to 6.8 m depth, and a stiff to very stiff silty clay layer between 6.8 m to 11.5 m depth with the water level at depth of 1 m (Bennett et al. 1984). Figure 16 illustrates Cross section and instrumentation of Wildlife downhole array site.

During the Superstition Hills 1987 earthquake, liquefaction occurred at the depth of 2.9 m within the silty sand layer and associated excess pore water pressure was measured by transducer P5 (at the depth of 2.9 m). The recorded EPWP data of transducer P5 in Fig. 17 shows that the excess pore water pressure reached the initial effective overburden stress near the end of seismic loading. This indicates that the imparted dissipated energy by the earthquake (demand energy) was just enough to trigger the liquefaction. In other words, the demand energy was a little greater than the capacity energy of the silty sand layer.

Zeghal and Elgamal (1994) analyzed the recorded acceleration data and calculated hysteresis loops at the depth of 2.9 m within the silty sand layer by estimating shear stress and strain histories. A similar procedure was used in this study to calculate hysteresis loops at the same depth for two orthogonal horizontal directions using both recorded acceleration components. Then, estimated cumulative dissipated energy at the depth of 2.9 m in conjunction with the recorded data of pore pressure transducer P5 was used to produce $r_u - W/W_{liq}$ diagram at the same depth within the silty sand layer (Fig. 18).

Correlation between SPT value and relative density is usually expressed as Eq. (11) which D_r, $N_{1,60}$, and C_d are relative density in percent, corrected SPT value for overburden pressure, and a constant factor, respectively. Many researchers suggested some values for C_d (e.g., Skempton 1986; Cubrinovski and Ishihara 1999; Idriss and Boulanger 2003) and in this study, $C_d = 46$ has been selected (Idriss and Boulanger 2003).

$$D_r = 100\sqrt{\frac{N_{1,60}}{C_d}} \tag{11}$$

Cetin et al. (2016) calculated $N_{1,60} = 6.5$ and $N_{1,60} = 7.8$ at the depth of 2.75 m and 3.35, respectively, for the wildlife site. By substituting the average value of $N_{1,60} = 7.1$ and $C_d = 46$ in Eq. (11), the relative density of 39% is obtained for the silty sand layer at the depth of 2.9 m. Also, the fines content of 34% is reported for the depth of 3.2 m.

By setting the $D_r = 39\%$ and $FC = 34\%$ in the proposed model, the predicted r_u values are presented in

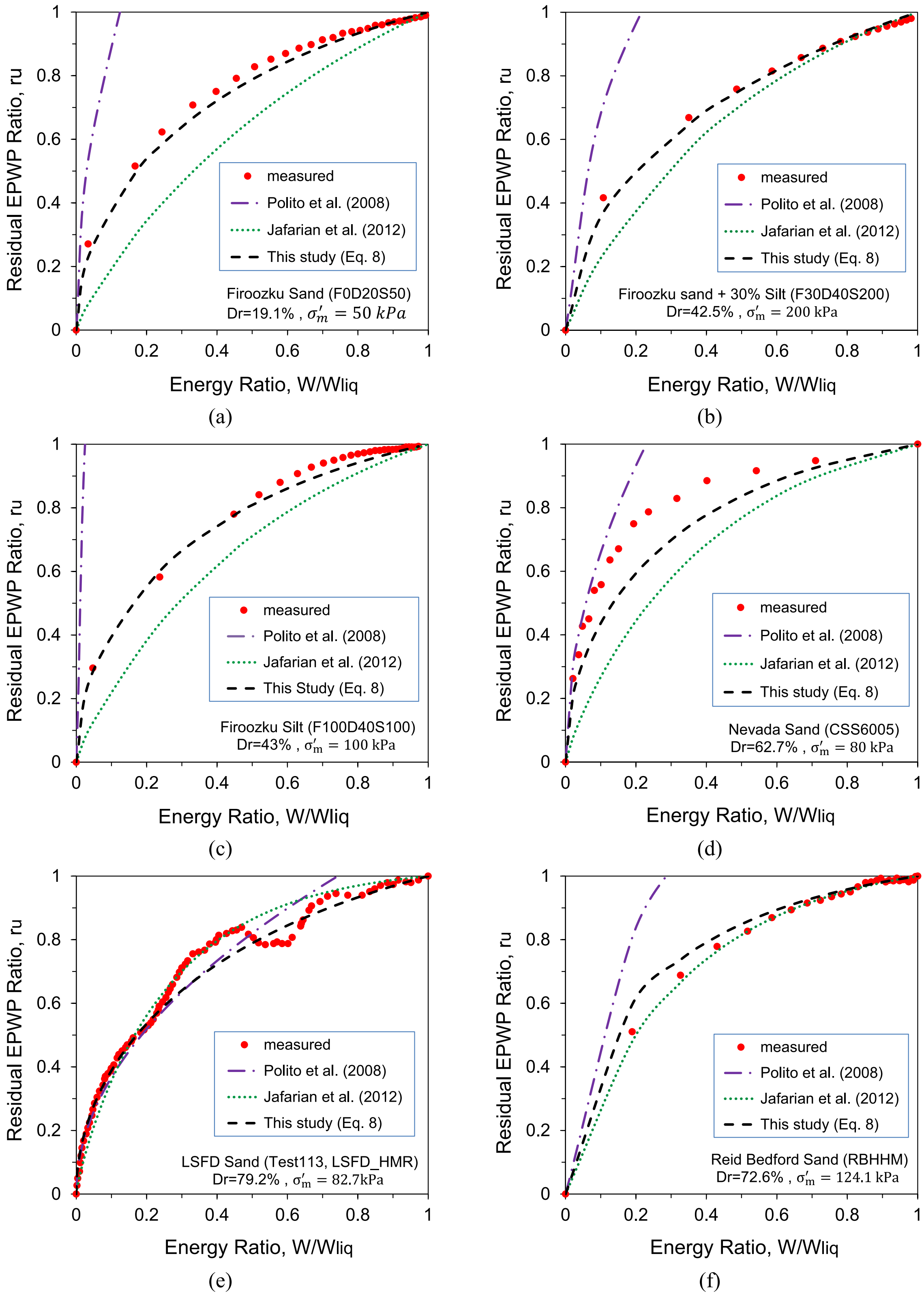
Residual EPWP Ratio, ru
Energy Ratio, W/Wliq
measured
Polito et al. (2008)
Jafarian et al. (2012)
This study (Eq. 8)
Firoozku Sand (F0D20S50)
Dr=19.1% , $\sigma'_m = 50\ kPa$
(a)
Firoozku sand + 30% Silt (F30D40S200)
Dr=42.5% , $\sigma'_m = 200$ kPa
(b)
Firoozku Silt (F100D40S100)
Dr=43% , $\sigma'_m = 100$ kPa
This Study (Eq. 8)
(c)
Nevada Sand (CSS6005)
Dr=62.7% , $\sigma'_m = 80$ kPa
(d)
LSFD Sand (Test113, LSFD_HMR)
Dr=79.2% , $\sigma'_m = 82.7$kPa
(e)
Reid Bedford Sand (RBHHM)
Dr=72.6% , $\sigma'_m = 124.1$ kPa
(f)

◂**Fig. 11** Measured and predicted values of r_u for **a** Firoozkuh sand (F0D20S50) at D_r = 19.1% and σ'_m = 50 kPa, **b** Firoozkuh sand +30%silt (F30D40S200) at D_r = 42.5% and σ'_m = 200 kPa, **c** Firoozkuh silt (F100D40S100) at D_r = 43% and σ'_m = 100 kPa, **d** Nevada sand (CSS6005) at D_r = 62.7% and σ'_m = 80 kPa, **e** LSFD sand (Test113, LSFD_HMR) at D_r = 79.2% and σ'_m = 82.7 kPa, **f** Reid Bedford sand (RBHHM) at D_r = 72.6% and σ'_m = 124.1 kPa

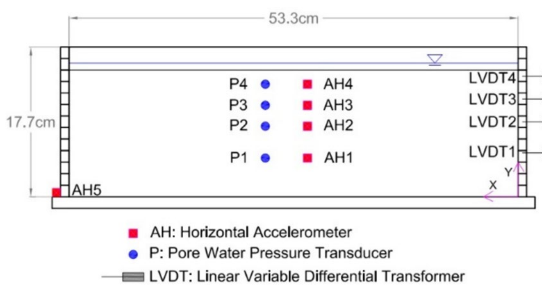

Fig. 12 Schematic illustration of laminar box, model configuration and instrumentation included in the soil (after Dief and Figueroa 2007)

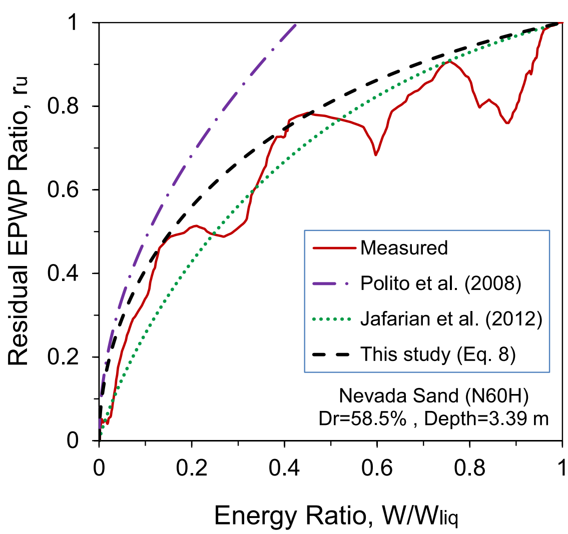

Fig. 13 Measured and predicted values of r_u versus energy ratio for centrifuge test of Nevada sand at depth of 3.39 m and D_r = 58.5%

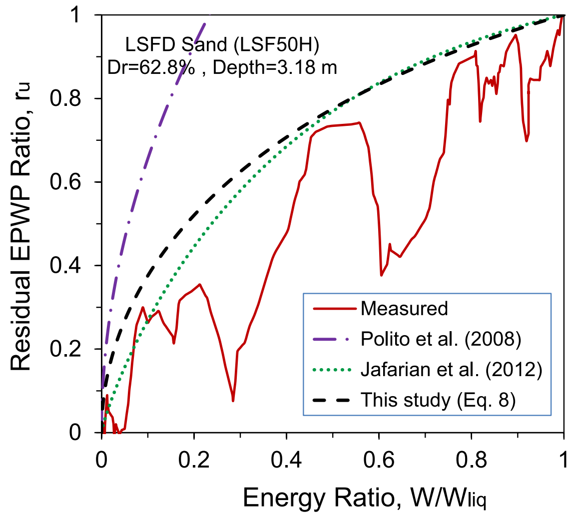

Fig. 14 Measured and predicted values of r_u versus energy ratio for centrifuge test of LSFD sand at depth of 3.18 m and D_r = 62.8%

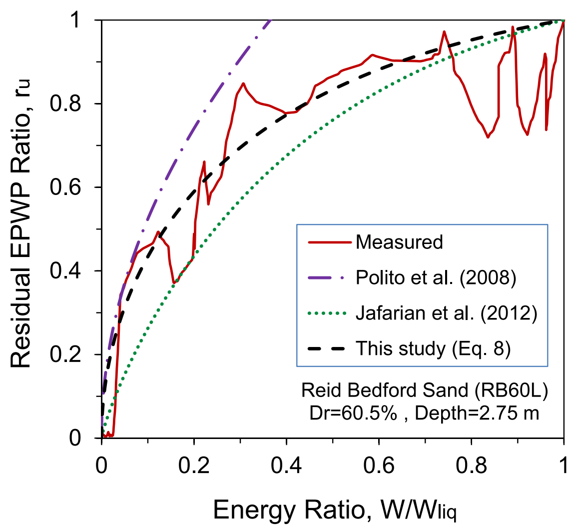

Fig. 15 Measured and predicted values of r_u versus energy ratio for centrifuge test of Reid Bedford sand at depth of 2.75 m and D_r = 60.5%

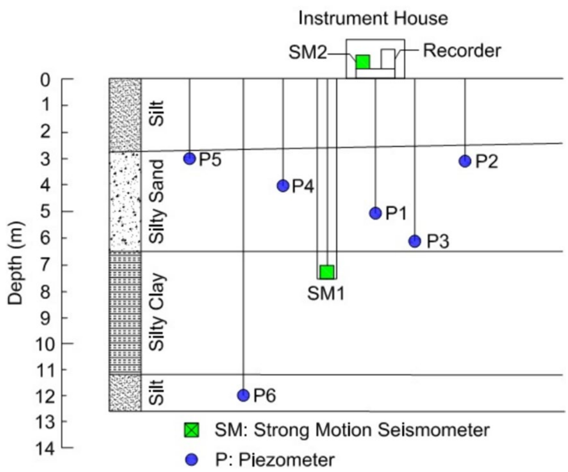

Fig. 16 Cross section and instrumentation of Wildlife downhole array site (after Zeghal and Elgamal 1994)

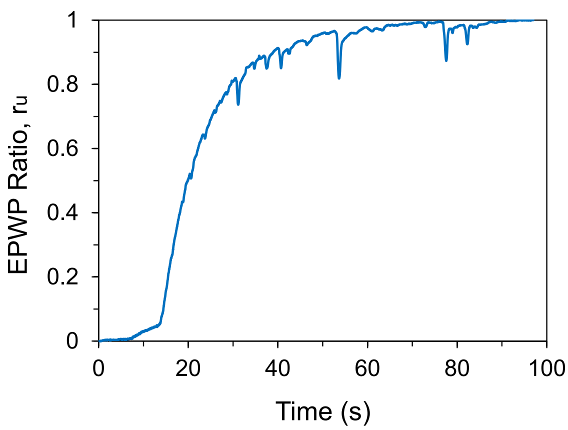

Fig. 17 Excess pore water pressure measured by transducer P5 (at depth of 2.9 m) during the Superstition Hills 1987 earthquake at Wildlife downhole array site

Fig. 18. According to this figure, there is a very good agreement between measured and predicted values. It confirms the suitable performance of the proposed model for real field conditions.

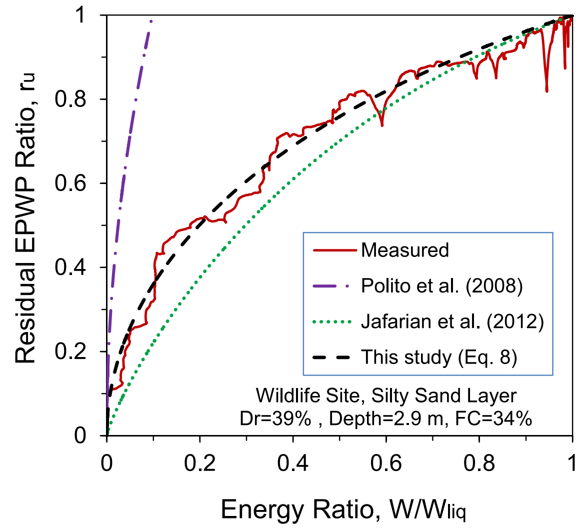

Fig. 18 Measured and predicted values of r_u versus energy ratio within the silty sand layer (at depth of 2.9 m) during the Superstition Hills 1987 earthquake at Wildlife downhole array site

7 Conclusions

In this paper, an energy-based model was developed for the prediction of residual excess pore water pressure generation during cyclic loading and was calibrated using a database of 72 cyclic tests. The proposed model has a simple mathematical form and has one calibration parameter of C. The C parameter is related to relative density and fines content. The model is practical and can be easily implemented in site response analysis for EBM liquefaction potential evaluation. Moreover, since this model directly relates the r_u to the factor of safety (FS), the r_u can be estimated using FS determined by an earthquake demand energy attenuation model (e.g., Baziar and Rostami 2017).

The proposed model was compared with results of centrifuge tests on three different soils simulating liquefaction of level ground sites and also Wildlife downhole array site recorded during the Superstition Hills 1987 earthquake and finally the efficiency of this model for predicting the pore water pressure generation induced by seismic loading was confirmed.

However, it should be mentioned that the EPWP model proposed in the present study has been developed and verified based on Siliceous clean sands and sand–silt mixtures with nonplastic fines content.

The applicability of the proposed model for sands with different origins (such as Calcareous sands) and mixtures with plastic fines content requires further investigations and developments and can be a matter of future studies.

Funding The authors declare that no funds, grants, or other support were received during the preparation of this manuscript.

Data availability The data and material presented here is available upon reasonable request from the corresponding author.

Declarations

Conflicts of interest The authors have no relevant financial or non-financial interests to disclose.

References

Akhila M, Rangaswamy K, Sankar N (2019) Undrained response and liquefaction resistance of sand–silt mixtures. Geotech Geol Eng 37(4):2729–2745. https://doi.org/10.1007/s10706-018-00790-0

Arulmoli K, Muraleetharan K, Hosain M, Fruth L (1992) VELACS laboratory testing program-soil data report. The Earth Technology Corporation, Irvine, Calif. Report to the National Science Foundation

Baziar MH, Jafarian Y (2007) Assessment of liquefaction triggering using strain energy concept and ANN model: capacity energy. Soil Dyn Earthq Eng 27(12):1056–1072. https://doi.org/10.1016/j.soildyn.2007.03.007

Baziar MH, Rostami H (2017) Earthquake demand energy attenuation model for liquefaction potential assessment. Earthq Spectra 33(2):757–780. https://doi.org/10.1193/030816eqs037m

Baziar MH, Shahnazari H, Sharafi H (2011) A laboratory study on the pore pressure generation model for Firouzkooh silty sands using hollow torsional test. Int J Civ Eng 9(2):126–134

Baziar MH, Shariatmadari N, Mohebbi HR, Mollahassani Lashkajani MH (2019) Comparing the liquefaction behavior of carbonate and silicate sands by energy approach. 8th Int. Conf. on Seismology and Earthquake Engineering,Tehran, Iran

Bennett M, McLaughlin P, Sarmiento J, Youd T (1984) Geotechnical investigation of liquefaction sites, Imperial Valley, California. Open-file Rep. 84–252. US Geological Survey, Washington, DC

Cetin KO, Seed RB, Kayen RE, Moss RE, Bilge HT, Ilgac M, Chowdhury K (2016) Summary of SPT based field case history data of cetin (2016) database. No. METU/GTENG 08/16-01. Middle East Technical University.

Chen G, Zhao D, Chen W, Juang CH (2019) Excess pore-water pressure generation in cyclic undrained testing. J Geotech Geoenviron Eng 145(7):04019022. https://doi.org/10.1061/(asce)gt.1943-5606.0002057

Cheng K, Zhang Y (2024) A cyclic resistance ratio model of sand-fines mixtures based on cyclic triaxial test. Geotech Geol Eng 42(2):1021–1033. https://doi.org/10.1007/s10706-023-02602-6

Cubrinovski M, Ishihara K (1999) Empirical correlation between SPT N-value and relative density for sandy soils. Soils Found 39(5):61–71. https://doi.org/10.3208/sandf.39.5_61

Dief HM, Figueroa JL (2007) Liquefaction assessment by the unit energy concept through centrifuge and torsional shear tests. Can Geotech J 44(11):1286–1297. https://doi.org/10.1139/t07-059

Dief HM (2000) Evaluating the liquefaction potential of soils by the energy method in the centrifuge. Ph.D. Dissertation, Case Western Reserve University

Dobry R, Ladd R, Yokel FY, Chung RM, Powell D (1982) Prediction of pore water pressure buildup and liquefaction of sands during earthquakes by the cyclic strain method. National Bureau of Standards, Gaithersburg

Doygun O, Brandes HG, Roy TT (2019) Effect of gradation and non-plastic fines on monotonic and cyclic simple shear strength of silica sand. Geotech Geol Eng 37(4):3221–3240. https://doi.org/10.1007/s10706-019-00838-9

Ghani S, Kumari S (2021) Insight into the effect of fine content on liquefaction behavior of soil. Geotech Geol Eng 39(1):1–12. https://doi.org/10.1007/s10706-020-01491-3

Ghorbani A, Eslami A (2021) Energy-based model for predicting liquefaction potential of sandy soils using evolutionary polynomial regression method. Comput Geotech 129:103867. https://doi.org/10.1016/j.compgeo.2020.103867

Gobbi S, Reiffsteck P, Lenti L, d'Avila MPS, Semblat J-F (2021) Liquefaction triggering in silty sands: effects of non-plastic fines and mixture-packing conditions. Acta Geotech 17(2):1–20. https://doi.org/10.1007/s11440-021-01262-1

Green R, Mitchell J, Polito C (2000) An energy-based excess pore pressure generation model for cohesionless soils. Proc. of the developments in theoretical geomechanics-the John Booker memorial symposium, Sydney, New South Wales, Australia

Green RA (2001) Energy-based evaluation and remediation of liquefiable soils. Ph.D. Dissertation, Virginia Polytechnic Institute and State University.

Hazirbaba K, Rathje EM (2009) Pore pressure generation of silty sands due to induced cyclic shear strains. J Geotech Geoenviron Eng 135(12):1892–1905. https://doi.org/10.1061/(asce)gt.1943-5606.0000147

Idriss I, Boulanger R (2003) Relating Kα and Kσ to SPT blow count and to CPT tip resistance for use in evaluating liquefaction potential. Proc. of the 2003 Dam Safety Conference, Lexington, Kentucky, USA

Ishihara K (1993) Liquefaction and flow failure during earthquakes. Geotechnique 43(3):351–451. https://doi.org/10.1680/geot.1993.43.3.351

Jafarian Y, Towhata I, Baziar M, Noorzad A, Bahmanpour A (2012) Strain energy based evaluation of liquefaction and residual pore water pressure in sands using cyclic

torsional shear experiments. Soil Dyn Earthq Eng 35:13–28. https://doi.org/10.1016/j.soildyn.2011.11.006
Kanth A, Bishoyi N, Kumar R (2024) Development of energy-based site-specific correlations to evaluate liquefaction potential. Geotech Geol Eng 42(3):1793–1809. https://doi.org/10.1007/s10706-023-02646-8
Kokusho T (2013) Liquefaction potential evaluations: energy-based method versus stress-based method. Can Geotech J 50(10):1088–1099. https://doi.org/10.1139/cgj-2012-0456
Kokusho T (2017) Liquefaction potential evaluations by energy-based method and stress-based method for various ground motions: Supplement. Soil Dyn Earthq Eng 95:40–47. https://doi.org/10.1016/j.soildyn.2017.01.033
Kokusho T, Kaneko Y (2018) Energy evaluation for liquefaction-induced strain of loose sands by harmonic and irregular loading tests. Soil Dyn Earthq Eng 114:362–377. https://doi.org/10.1016/j.soildyn.2018.07.012
Kokusho T, Tanimoto S (2021) Energy capacity versus liquefaction strength investigated by cyclic triaxial tests on intact soils. J Geotech Geoenviron Eng 147(4):04021006. https://doi.org/10.1061/(asce)gt.1943-5606.0002484
Ladd R (1978) Preparing test specimens using undercompaction. Geotech Test J 1(1):16–23. https://doi.org/10.1520/gtj10364j
Liang L (1995) Development of an energy method for evaluating the liquefaction potential of a soil deposit. Ph.D. Dissertation, Case Western Reserve University.
Liu J (2020) Influence of fines contents on soil liquefaction resistance in cyclic triaxial test. Geotech Geol Eng 38(5):4735–4751. https://doi.org/10.1007/s10706-020-01323-4
Nemat-Nasser S, Shokooh A (1979) A unified approach to densification and liquefaction of cohesionless sand in cyclic shearing. Can Geotech J 16(4):659–678. https://doi.org/10.1139/t79-076
Polito CP, Green RA, Lee J (2008) Pore pressure generation models for sands and silty soils subjected to cyclic loading. J Geotech Geoenviron Eng 134(10):1490–1500. https://doi.org/10.1061/(asce)1090-0241(2008)134:10(1490)
Polito CP (1999) The effects of non-plastic and plastic fines on the liquefaction of sandy soils. Ph.D. Dissertation, Virginia Polytechnic Institute and State University.
Porcino DD, Diano V (2017) The influence of non-plastic fines on pore water pressure generation and undrained shear strength of sand–silt mixtures. Soil Dyn Earthq Eng 101:311–321. https://doi.org/10.1016/j.soildyn.2017.07.015
Porcino D, Diano V, Triantafyllidis T, Wichtmann T (2020) Predicting undrained static response of sand with non-plastic fines in terms of equivalent granular state parameter. Acta Geotech 15(4):867–882. https://doi.org/10.1007/s11440-019-00770-5
Rahman MM, Lo S, Gnanendran C (2008) On equivalent granular void ratio and steady state behaviour of loose sand with fines. Can Geotech J 45(10):1439–1456. https://doi.org/10.1139/t08-064
Sezer A, Kumasdere C, Tanrinian N, Karakan E (2024) Energy-based assessment of liquefaction behavior of a non-plastic silt based on cyclic triaxial tests. Turk J Civ Eng 35(3):71–94. https://doi.org/10.18400/tjce.1283189
Skempton A (1986) Standard penetration test procedures and the effects in sands of overburden pressure, relative density, particle size, ageing and overconsolidation. Geotechnique 36(3):425–447. https://doi.org/10.1680/geot.1986.36.3.425
Sonmezer YB (2019) Energy-based evaluation of liquefaction potential of uniform sands. Geomech Eng 17(2):145. https://doi.org/10.12989/gae.2019.17.2.145
Tao M (2003) Case history verification of the energy method to determine the liquefaction potential of soil deposits. Ph.D. Dissertation, Case Western Reserve University.
Wang G, Takemura J, Kuwano J (1997) Evaluation of excess pore water pressures of intermediate soils due to cyclic loading by energy method. In: Proceedings of the 9th international conference of international Association for Computer Method and Advances in Geomechanics, Wuhan, China
Yanagisawa E, Sugano T (1994) Undrained shear behaviors of sand in view of shear work. In: Proceedings of the 13th international conference on soil mechanics and foundation engineering (Special Volume on Performance of Ground and Soil Structures during Earthquakes), New Delhi, India
Yang Z, Pan K (2018) Energy-based approach to quantify cyclic resistance and pore pressure generation in anisotropically consolidated sand. J Mater Civ Eng 30(9):04018203. https://doi.org/10.1061/(asce)mt.1943-5533.0002419
Yang S, Lacasse S, Sandven R (2006) Determination of the transitional fines content of mixtures of sand and non-plastic fines. Geotech Test J 29(2):102–107. https://doi.org/10.1520/gtj14010
Yazdani E, Nguyen A, Evans TM (2022) Shear-induced instability of sand containing fines: using the equivalent intergranular void ratio as a state variable. Int J Geomech 22(8):04022121. https://doi.org/10.1061/(asce)gm.1943-5622.0002486
Zeghal M, Elgamal A-W (1994) Analysis of site liquefaction using earthquake records. J Geotech Eng 120(6):996–1017. https://doi.org/10.1061/(asce)0733-9410(1994)120:6(996)
Zhou G, Pan K, Yang Z (2023) Energy-based assessment of cyclic liquefaction behavior of clean and silty sand under sustained initial stress conditions. Soil Dyn Earthq Eng 164:107609. https://doi.org/10.1016/j.soildyn.2022.107609